Echinocyte Shapes: Bending, Stretching, and Shear Determine Spicule Shape and Spacing

Ranjan Mukhopadhyay, Gerald Lim H. W., and Michael Wortis
Department of Physics, Simon Fraser University Burnaby, British Columbia, V5A 1S6 Canada

ABSTRACT   We study the shapes of human red blood cells using continuum mechanics. In particular, we model the crenated, echinocytic shapes and show how they may arise from a competition between the bending energy of the plasma membrane and the stretching/shear elastic energies of the membrane skeleton. In contrast to earlier work, we calculate spicule shapes exactly by solving the equations of continuum mechanics subject to appropriate boundary conditions. A simple scaling analysis of this competition reveals an elastic length Λ_{el}, which sets the length scale for the spicules and is, thus, related to the number of spicules experimentally observed on the fully developed echinocyte.

INTRODUCTION

The normal resting shape of the human red blood cell (RBC or erythrocyte) is a flattened biconcave disc (discocyte) $\sim$8 μm in diameter. Treatment of erythrocytes in vitro with a variety of amphipathic agents is known to transform this shape systematically and reversibly into various other shapes such as echinocytes (crenated shapes) and stomatocytes (cup-like shapes), which are further subdivided into classes labeled I, II, and III (Brecher and Bessis, 1972; Bessis, 1973; Chailley et al., 1973; Mohandas and Feo, 1975). In particular, the echinocyte III is a more-or-less spherical body covered evenly with 25 to 50 rounded protuberances, which we shall call spicules.

These shape transformations—from the discocyte to the stomatocyte on one side and from the discocyte to the echinocyte on the other—have been studied experimentally for more than 50 years. Understanding these shapes and shape transformations is a classic problem in cell biology; over the past three decades it has also attracted the attention of physicists. What makes this problem so intriguing is that the structure of the red cell is remarkably simple. To a good approximation it is simply a bag of fluid, a concentrated solution of hemoglobin surrounded by a thin macroscopically homogeneous membrane. Thus, the diverse resting shapes that it exhibits can be thought of as (locally) stable mechanical equilibrium shapes of the membrane. This membrane is composite (Steck, 1989; Alberts et al., 1994). On the outside is the plasma membrane, a self-assembled fluid bilayer with a thickness of $\sim$4 nm, composed of a complex mix of phospholipids, cholesterol, and dissolved proteins. Lipids such as phosphatidylcholine, sphingomyelin, and glycophospholipids, which are neutral at physiological pH, are common in the outer leaflet, whereas phosphatidylserine and phosphatidylethanolamine predominate in the inner leaflet (Gennis, 1989; Alberts et al., 1994). Due to the negative charge of phosphatidylserine, located in the inner leaflet, there is a significant difference in charge between the two leaflets of the bilayer. Inside the plasma membrane but linked to it by protein anchors is a thin, two-dimensionally cross-linked protein cytoskeleton, the membrane skeleton (Steck, 1989; Bennett, 1990). The skeleton is an hexagonally linked net, each unit of which is a filamentous spectrin tetramer with an extended length of $\sim$200 nm; the end-to-end distance is reduced appreciably in the relaxed state by thermal fluctuations (Boal, 1994). The spectrin tetramer is negatively charged at physiological pH. In the red cell membrane, the distance between the vertices of the net is $\sim$76 nm, whereas the offset between the plasma membrane and the spectrin network is 30 to 50 nm (Byers and Branton, 1985; Liu et al., 1987). Functionally, the plasma membrane serves as an osmotic barrier, passing water with relative ease but controlling, via a system of pumps and channels, the flow of ions and larger solute molecules. The membrane skeleton has the role of supporting and toughening the plasma membrane, which would otherwise disintegrate in circulatory shear flow.

Although the RBC membrane is certainly heterogeneous at the length scale of individual lipid molecules, lipid patches or the basic spectrin tetramer, on scales longer than 100 nm it is reasonably homogeneous in its properties, and it may make sense to treat it as a mechanical continuum. In this spirit and following early work by Canham (1970), Helfrich (Helfrich, 1973; Deuling and Helfrich, 1976), and others, we imagine replacing the (fluid-phase) plasma membrane by an ideal uniform two-dimensional surface characterized by a bending rigidity κ_b, taken for the RBC to be (Waugh and Bauserman, 1995; Strey et al., 1995) 2.0 $\times$ 10^{-19} J (roughly 50 $k_B T_{room}$, where k_B is Boltzmann's constant), a spontaneous curvature C_0, which recognizes the outside-inside asymmetry of the leaflet composition, and an area-difference-elasticity (ADE) term (Helfrich, 1973; Evans, 1974; Svetina et al., 1985; Božič et al., 1992; Wiese et al., 1992; Miao et al., 1994), which reflects the fact that a difference in relaxed area, ΔA_0, between the outer and

inner leaflets produces a "bilayer couple" (Sheetz and Singer, 1974) tending to make the membrane become convex with the larger-area side on the outside of the convexity (like a bimetallic strip). We assign to the modulus $\bar{\kappa}$ associated with the ADE term a value of (Waugh and Bauserman, 1995) 1.27×10^{-19} J. These terms taken together constitute what is called the ADE model of the plasma membrane. In addition, we represent the RBC membrane skeleton as a two-dimensional elastic continuum characterized by a bulk stretching modulus K_α and a shear modulus μ with $\mu \approx 2.5 \times 10^{-6}$ J/m^2 and $K_\alpha \approx 3 \mu$ (see Discussion). These two mechanical subsystems, constrained to the same mathematical surface, will constitute our model of the RBC shape at length scales above 100 nm (for full details, see The Model).

The basic hypothesis of the mechanical approach is that the observed RBC shapes must be shapes that minimize the energy subject to appropriate constraints on volume and area, i.e., that all the observed RBC shapes must emerge as local energy minima of this model and that the observed shape transformations must come about as a response of the minimum-energy shapes to changes in the "control parameters," which characterize the model. There are relatively few such control parameters. In addition to the known area and volume of the RBC, we include in the list the three mechanical moduli noted above, the spontaneous curvature C_0, the relaxed area difference ΔA_0 between the bilayer leaflets, and parameters describing the effective relaxed size and shape of the membrane skeleton. If all these control parameters were known or easily measurable, we could predict the stable RBC shapes using continuum mechanics. The fact that they are not restricts us, as we shall see, to somewhat more generic predictions.

This program has already been carried out, albeit in somewhat restricted form, with respect to the discocyte and stomatocyte shapes. The shapes and shape transitions of laboratory-prepared fluid-phase phospholipid vesicles (lacking any skeleton) have been successfully described by the ADE model (Miao et al., 1994; Döbereiner et al., 1997). In particular, plausible discocytic and stomatocytic shapes do occur as energy-minimizing shapes of the ADE model. Furthermore, the bilayer-couple mechanism (Sheetz and Singer, 1974) accounts qualitatively for many of the chemically induced discocyte-stomatocyte transitions observed in the laboratory, in that stomatocytogenic agents tend to segregate to the inner leaf of the bilayer, thus making ΔA_0 negative and favoring the invaginated stomatocyte shape (see more below). There has been discussion in the literature of the way in which introducing the elastic energy of the membrane skeleton modifies or improves the detailed prediction for the shape of the normal resting discocyte (Zarda et al., 1977; Evans and Skalak, 1980). However, most treatments in the literature tend to regard the cytoskeletal elastic energy as providing only perturbative modification of the basic shapes, which emerge from the pure-bending-
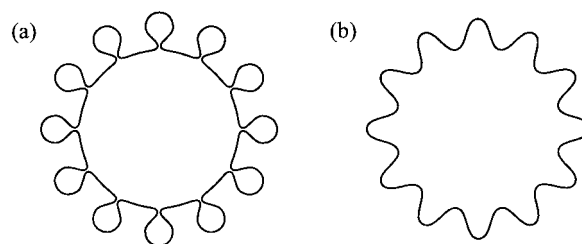

FIGURE 1   (a) Budded or vesiculated shape, which would be a low-energy configuration of a lipid membrane without cytoskeleton at sufficiently positive spontaneous curvature. (b) Spiculated shape into which (a) is transformed by the elastic-energy cost of cytoskeletal deformations in the high-shear neck regions.

energy model. We shall argue that this point of view fails completely in describing echinocyte shapes.

Until recently, it was a major difficulty for a fully mechanical picture of the RBC shapes that echinocytic shapes have not been found in the catalog of minimum-energy shapes of the ADE model; however, several authors have now pointed out what we believe is the correct resolution of this problem (Waugh, 1996; Iglič, 1997; Iglič et al., 1998a,b; Wortis, 1998). A pure-lipid vesicle with a sufficiently positive spontaneous curvature (or, equivalently, sufficiently large positive ΔA_0) adopts a vesiculated or budded shape, in which one or more quasispherical buds appears on the outside of the main body of the vesicle, attached to it via a narrow neck or necks (Fig. 1). Such necks are allowed as low-energy structures for pure-lipid vesicles, because the bending energy depends on the sum of the two principal curvatures (see The Model), so that large curvatures of opposite sign (characteristic of necks) can still lead to a small mean curvature and, thus, to low energy (Fourcade et al., 1994). But (and this is the crucial point) small necks involve large elastic strains in the membrane skeleton and are, thus, inhibited by elastic energy cost. It is not surprising that they are not seen for undamaged RBCs. What our calculations show is that the formation of echinocytes is driven by positive C_0 (equivalently, positive ΔA_0) and that the spiculated shapes seen in experiments can arise from a competition between the bending energy of the plasma membrane, which by itself would promote budding, and the stretching and shear elastic energies of the membrane skeleton, which prevent it. To make this more precise, we note that the ratio of the bending modulus to the shear modulus (or the stretching modulus) defines an elastic length scale,

$$\Lambda_{\mathrm{el}} = \sqrt{\frac{\kappa_{\mathrm{b}}}{\mu}}, \qquad (1)$$

which yields $\Lambda_{\mathrm{el}} \approx 0.28 \ \mu$m. We shall see below that this number sets the scale of spicule size and, thus, fixes the spicule density of the fully developed echinocyte (echinocyte III).

The success of this approach strengthens the hypothesis that RBC shapes can be understood on the basis of continuum mechanics; however, in themselves, such calculations cannot answer the question, "Why does a particular shape occur under given experimental conditions?" Such a question has two parts. Why do the control parameters have the values they do? How does this set of control parameters lead to the observed shape? The second part is the proper domain of continuum mechanics. The first part is primarily biological or biochemical in content and revolves around the mechanisms that control the lipid composition of the leaflets of the plasma membrane, local electrostatic effects, the composition and environment of the spectrin network, and its coupling to the plasma membrane, and any other determinants of C_0, ΔA_0, the elastic moduli, and other control parameters. Hopefully, this separation of the question is useful.

The plan of this paper is as follows. In the remainder of this section, we briefly review some history of echinocyte shapes and shape calculations. The Model section presents the details of the continuum-mechanics model. Theory section discusses the theory required to solve the model numerically for echinocyte shapes, including a full account of the scaling argument suggested above. The Results section presents our results for the predicted echinocyte shapes and spicule density. The Discussion section contains discussion of our results and further speculations.

The discocyte-to-echinocyte transformation was precisely identified by Ponder (1948, 1955) and has since been studied extensively by many other authors, as reviewed, for example, by Bessis (1973), Lange et al. (1982), and Steck (1989). Although this transformation can be driven in many ways, the final spiculated shapes produced are apparently the same (Smith et al., 1982; Mohandas and Feo, 1975). This quasi-universal behavior is evidence for the kind of mechanism suggested above, in which quite diverse biochemical processes may set (a few) important control parameters to the same or similar values. In the same spirit, we note that RBC ghosts (formed by hemolysis) behave quite similarly to intact red cells (Lange et al., 1982).

The simplest picture of this type—consistent with some (but not necessarily all) experimental findings—is the so-called bilayer-couple hypothesis of Sheetz and Singer (1974), which focuses attention on the control parameter ΔA_0. Thus, adding exogenous phospholipids to the exterior solution is observed to promote echinocyte formation (Ferrell et al., 1985; Christiansson et al., 1985). This is explained in the bilayer-couple picture by arguing that such addition is expected to produce an area increase in the outer leaflet only, as phospholipids do not readily flip-flop from one leaflet to the other. This increases the area difference ΔA_0 and is expected to promote echinocyte formation. Similarly, cholesterol does equilibrate across the bilayer but apparently prefers the outer leaflet, presumably because of the particular lipids there present. Thus, adding cholesterol

will tend to increase ΔA_0 and promote echinocytosis, whereas depleting cholesterol will tend to decrease ΔA_0 and to promote stomatocytosis (Lange and Slayton, 1982). More generally, anionic amphipaths all tend to produce echinocytes, whereas cationic amphipaths tend to produce stomatocytes (Deuticke, 1968; Weed and Chailley, 1973; Mohandas and Feo, 1975; Smith et al., 1982). The bilayer-couple explanation of these observations is that, when incorporated into the plasma membrane, the cationic compounds segregate preferentially to the inner leaflet and the anionic compounds, to the outer leaflet because of the predominantly negative charge of the inner-leaflet lipids. Outer-leaflet segregation increases ΔA_0, thus promoting echinocytosis; conversely, inner-leaflet segregation promotes stomatocytosis. Time-dependent effects have even been seen, where a molecule initially intercalates into the outer leaflet, causing echinocytosis, but then slowly migrates to the inner leaflet, following the electrostatic gradient, causing return to the discocyte and subsequent stomatocytosis (Isomaa et al., 1987).

A similar hypothesis is made to explain the observed tendency of ghosts to become echinocytes at high salt concentrations but stomatocytes at low salt concentrations (Lange et al., 1982). The argument relies on electrostatics. Cationic species neutralize the negative lipid charges on the inner leaflet and salt decreases the Debye length, more effectively screening such charges. Both effects lead to a contraction of the inner leaflet and consequent increase in ΔA_0, promoting crenation.

Other observations can be linked to the bilayer-couple effect but somewhat less directly. Thus, it is found that hemolyzed echinocytes produce discocytic ghosts (Lange et al., 1982) and that electroporation suppresses shape changes (Schwarz et al., 1999a,b). To explain these effects, it is argued that hemolysis and electroporation both involve perforation of the membrane and resulting in contact via the pore surface between the lipids in the inner and outer leaflets. This provides a mechanism for lipid transport that may reduce the magnitude of ΔA_0 by partial symmetrization of the lipid composition of the leaflets, thus (equivalently) reducing C_0. Similarly, it is known that ATP depletion drives discocytes to crenate (Nakao et al., 1960, 1961, 1962; Backman, 1986). The hypothesis here is that ATP is required in some way to maintain the lipid asymmetry of the leaflets (related to C_0), perhaps for the operation of ATP-driven translocases (Steck, 1989).

Some effects are not readily explained by the bilayer-couple mechanism. Weed and Chailley (1972) and Gedde et al. (1995, 1997a,b, 1999) report that RBC shape can be controlled experimentally by varying the external pH with high pH promoting echinocyte formation and low pH, stomatocyte formation (the effect of proximity to a glass surface in promoting echinocytosis (Furchgott and Ponder, 1940) is probably related to this effect). The mechanism for this effect does not seem to be well established. Some

authors argue for a mechanism involving membrane proteins. Band 3 has been specifically implicated (Gimsa and Ried, 1995; Jay, 1996; Gimsa, 1998; Hägerstrand et al., 2000). For example, it is known that high pH induces dissociation of ankyrin and band 3, which plays a role in the linkage of the membrane skeleton to the bilayer (Low et al., 1991). Indeed, it was shown that in vitro the membrane skeleton expands at high pH and contracts at low pH (Elgsaeter et al., 1986; Stokke et al., 1986). It has recently been proposed that pH change may induce conformational transformation in band 3 protein, leading to a change in ΔA_0. Similarly, Wong (1994, 1999) has proposed that the folding of the spectrin in the cytoskeletal net is controlled by a conformational change of the band 3 protein. Such mechanisms might shift the emphasis of shape determination from the dominantly lipid-related control parameters, C_0 and ΔA_0, to the elastic parameters and the relaxed shape of the membrane skeleton. We shall comment briefly on these issues in the Discussion section.

Numerous shape calculations have previously been done using variants of the model we describe in The Model. Early calculations (Fung and Tong, 1968; Zarda et al., 1977; Evans and Skalak, 1980) omitted the ADE term ($\bar{\kappa} = 0$), set $C_0 = 0$, and concentrated entirely on the shape of the resting discocyte and the modifications caused by osmotic swelling. They solved numerically the full mechanical shape equations. Landman (1984) treated a viscoelastic shell surrounding a viscous droplet and modeled the formation of protrusions as sudden local addition of shell material. Waugh (1996) studied a full ADE model with local shear elasticity (but treating the compressibility modulus as infinite) and studied the instability of a flat membrane to formation of a local "bump" (axisymmetric spicule) for positive values of C_0 or ΔA_0 or both. He assumed a specific spicule-shape parametrization, focussed on a single spicule, calculated its energy, and in this way was able to discuss generically the conditions under which spicule formation might become energetically favorable. Most recently, Iglič and collaborators (Iglič, 1997; Iglič et al., 1998a,b) have used the same model as Waugh (1996) but parametrize the spicule more simply, using a hemispherical cap on a cylindrical body and joining this to a spherical surface via a base shaped like a toroidal section. They correctly identify the emergence of echinocyte shapes as a competition between the bending energy and the skeletal elasticity. They model the echinocyte as a collection of n_s spicules attached to a spherical body and then determine the radius of the sphere, the parameters of the spicules, and the preferred number of spicules by minimizing the mechanical energy subject to constraints on cell area and volume. In this way, they are able to estimate the expected number of spicules and their shape as a function of the relaxed area difference ΔA_0.

The present paper builds on the work of Waugh (1996) and Iglič (1997, 1998a,b). We extend the model to include the area modulus K_α of the membrane skeleton. We calculate spicule shape for the first time from the Euler-Lagrange equations (these calculations are closely related to the earlier work of Zarda et al. (1977)). Although we continue with Iglič et al. (1998a,b) to treat the echinocyte as a sphere decorated with spicules, we deal seriously (although still approximately) with the mechanical boundary conditions that must be met where the spicule joins the sphere.

THE MODEL

The central assumption of our work is that the red blood cell assumes a shape that minimizes its overall membrane energy subject to the appropriate constraints. The RBC membrane is a composite of the plasma membrane and the cytoskeletal network; correspondingly, we take the membrane energy to be a sum of two terms,

$$F = F_b + F_{el}, \qquad (2)$$

the bending energy,

$$F_b = \frac{1}{2}\kappa_b \int dA(C_1 + C_2 - C_0)^2 + \frac{\bar{\kappa}}{2}\frac{\pi}{AD^2}(\Delta A - \Delta A_0)^2, \qquad (3)$$

associated with the bilayer and an elastic energy of stretching and shear,

$$F_{el} = \frac{1}{2}K_\alpha \int dA_0(\lambda_1\lambda_2 - 1)^2 + \frac{\mu}{2}\int dA_0\left(\frac{\lambda_1}{\lambda_2} + \frac{\lambda_2}{\lambda_1} - 2\right), \qquad (4)$$

associated with the skeleton. In doing this, we treat the plasma membrane as incompressible. An estimate of its stretching modulus is $K_\alpha^{(bilayer)} \sim 10^{-1}$ J/m², comparable with that of a pure-phospholipid bilayer and some four orders of magnitude larger than that of the skeleton. Correspondingly, we ignore any bending rigidity associated with the isolated membrane skeleton (the dimensional estimate $\kappa_b^{(skeleton)} \sim K_\alpha \times$ (thickness)² leaves it two orders of magnitude smaller than that of the bilayer).

Eq. 3 for the plasma membrane's contribution to the overall membrane energy is the now-standard ADE Hamiltonian (Svetina et al., 1985; Božič et al., 1992; Wiese et al., 1992; Miao et al., 1994). The first term was originally proposed by Helfrich (Helfrich, 1973; Deuling and Helfrich, 1976). C_1 and C_2 are the two local principal curvatures, C_0 is the spontaneous curvature, and the integral is over the membrane surface. The two leaves of a closed bilayer of

fixed interleaflet separation D are required by geometry to differ in area by an amount,

$$\Delta A = D \int dA (C_1 + C_2). \tag{5}$$

In calculations, we shall take $D \approx 3$ nm, corresponding to the distance between the neutral surfaces of the leaflets. The second term in Eq. 3 is the so-called area-difference-elasticity energy and represents the cost in stretching (or compressional) energy of the individual leaflets necessary to force the change from the relaxed area difference ΔA_0 so as to conform to this geometric requirement. This effect occurs because a strong hydrophobic barrier prevents lipids in one leaflet from "flip-flopping" passively to the other on the time scales of mechanical shape changes. A is the area of the plasma membrane. The modulus $\bar{\kappa}$ associated with the ADE term is generically of the same scale as κ_b. Note, finally, that we can substitute Eq. 5 to rewrite Eq. 3,

$$F_b = \frac{1}{2} \kappa_b \left[\int dA (C_1 + C_2)^2 + \frac{\pi \alpha}{A} \left(\int dA (C_1 + C_2) \right)^2 \right.$$
$$\left. - 2 \bar{C}_0 \int dA (C_1 + C_2) \right] + \text{const.}, \tag{6}$$

in which

$$\bar{C}_0 = C_0 + \frac{\pi \alpha \Delta A_0}{DA}, \tag{7}$$

$\alpha = \bar{\kappa}/\kappa_b$, and the constant term is shape independent. This shows that, in determining minimal shapes at given values of the control parameters, C_0 and ΔA_0 do not enter independently but only in the form of an effective spontaneous curvature $\bar{C}_0$ or, equivalently, an effective relaxed area difference,

$$\overline{\Delta A_0} = \Delta A_0 + \frac{DA C_0}{\pi \alpha}, \tag{8}$$

which we shall often quote in the dimensionless, reduced form

$$\overline{\Delta a_0} = \frac{\overline{\Delta A_0}}{A} = \Delta a_0 + \frac{D C_0}{\pi \alpha}. \tag{9}$$

Note for future reference that increasing Δa_0 by 0.01 is equivalent to increasing C_0 by 6.7 μm^{-1}.

Eq. 4 measures the elastic-energy cost of the spectrin network. It depends both on the relaxed shape of the membrane skeleton and on the way it is actually distributed over the membrane surface. (The notion of a relaxed shape is, of course, somewhat nominal, because removing the skeleton from the plasma membrane—which can certainly be done (Sheetz, 1979)—would radically change its local biochem-

ical environment, in a way which would modify its shape and elastic constants). In this redistribution, each element of the network will be stretched or compressed. The quantities λ_1 and λ_2 are the local principal extension ratios of each membrane element (Evans and Skalak, 1980). K_α and μ are the (two-dimensional) moduli for stretch and shear, respectively, as introduced in the Introduction, and the integrals are over the undeformed shape. In writing Eq. 4, we are assuming, as appears to be typical, that the membrane skeleton does not plastically deform in the course of the experimental shape transformation being described. Note that Eq. 4 makes a particular choice of terms in the elasticity beyond those quadratic in the weak-deformation parameters, $\epsilon_i = \lambda_i - 1$. For the large elastic strains, which are present at narrow necks and for small spicules, these nonlinearities do play a role. As far as we are aware, RBC elasticity has not been measured well enough to produce a clear preference for a particular form of the nonlinearities. Various authors have used Eq. 4 for the elastic energy in other contexts with apparent success; however, alternative forms of the elasticity have also been proposed for dealing with problems involving large local deformations (Evans and Skalak, 1980; Discher et al., 1994). We shall make some additional comments in the Discussion.

One attractive feature of Eq. 4 is that the effect of changing the size of the relaxed membrane skeleton by a pure, uniform dilation is particularly simple. Suppose that the skeleton is decreased in linear scale by a factor b. This means that undeformed areas are reduced by a factor $1/b^2$, whereas the extension ratios $\lambda_{1,2}$ are each increased by a factor b. Note that the integrand of the shear term in Eq. 4 is invariant under this change but the factor $\lambda_1 \lambda_2$ in the stretching integrand increases by b^2. Only the quadratic part of the stretching term influences the membrane shape because $\int dA_0 \lambda_1 \lambda_2$ is just the membrane area A, which is fixed by the incompressibility of the plasma membrane. It follows that the effect of decreasing the size of the skeleton is completely equivalent to keeping the size fixed but, instead, changing the elastic moduli according to

$$K_\alpha' = b^2 K_\alpha \tag{10}$$

$$\mu' = b^{-2} \mu, \tag{11}$$

i.e., this "prestress" in the membrane skeleton is completely equivalent to no prestress, a harder stretching modulus, and a softer shear modulus. It is not known with certainty what "prestress" exists in the typical RBC skeleton. Computer simulation has suggested that the relaxed skeleton may be as much as 10 to 20% smaller in area than the plasma membrane (Boal, 1994). On the other hand, the experiment by Svoboda et al. (1992) shows that isolated skeletons are expanded. In our calculations, we shall assume zero net prestress (relaxed skeletal area equal to RBC area, i.e., $\gamma \equiv A/A_0 = 1$). Any deviation from this would result in modified, effective elastic constants according to Eqs. 10 and 11.

In our calculations, we will identify shapes that are minima of the (free) energy defined by Eqs. 2 through 4 subject to constraints of fixed membrane area A (bilayer incompressibility) and volume V (as the RBC volume is typically set by osmotic balance). Constrained minimization is achieved variationally by introducing the functional,

$$\Phi(\Sigma, P) = F + \Sigma A - PV, \qquad (12)$$

in which Σ and P are Lagrange multipliers used to enforce the surface-area and volume constraints. P is the pressure difference across the bilayer, whereas Σ has the dimension of a surface tension. Making Φ stationary with respect to variations of membrane shape and cytoskeletal distribution leads to a set of coupled Euler-Lagrange equations. These equations can then be solved to give the shapes of mechanical equilibrium. In principle, such shapes are expected to correspond to observed equilibrium shapes at temperature $T = 0$ only; however, because the energy scale κ_b is large on the scale of k_BT, thermal fluctuations are generally negligible and play an important role only for "soft" modes, especially near instabilities (Wortis et al., 1997). The Euler-Lagrange equations are in general nonlinear and can have multiple solutions. The lowest-energy solution for given A and V is automatically stable to small fluctuations; higher-energy solutions must be tested for stability. All local-minimum solutions are candidates for stable observable shapes, except in exceptional cases (near instability) where energy barriers become comparable to k_BT.

The stable shapes produced by this process depend on the control parameters: the geometrical parameters, A and V; the determinants of curvature, C_0 and ΔA_0, which only enter in the combination found in Eq. 7 or equivalently, Eqs. 8 and 9, the moduli, κ, $\bar{\kappa}$, K_α, and μ; plus, finally, any parameters required to characterize the relaxed shape of the membrane skeleton. The area and volume of a typical RBC we take as (Bessis, 1973) $A = 140~\mu m^2$ and $V = 90~\mu m^3$. The moduli, given in the Introduction, are less well determined by experiment (we shall have more to say on this point in the Discussion Section). This leaves as unknown control parameters the curvature variables and the cytoskeletal parameters.

The Euler-Lagrange variational equations derived from (12) are not numerically tractable except in the case of axisymmetry, which clearly does not apply to echinocytic shapes. In this paper, we aim to treat only fully developed echinocytic shapes (echinocyte III). For this case, individual spicules are identical and axisymmetric in shape to a good approximation and, in addition, the central body, which they decorate is approximately spherical with radius R_0. The observed distribution of spicules is rather regular, and we shall approximate the local spicule packing as a triangular array (except for special numbers of spicules, there must, of course, be some defects), which will look increasingly like an hexagonal close-packed structure, as the number of spicules, n_s, becomes large.

The base of each individual spicule, where it meets the sphere tangentially, is a circular contour L of radius r_L. If θ_L is the angle subtended by L at the center of the sphere, then

$$r_L = R_0 \sin \theta_L. \qquad (13)$$

Because of the close-packed structure, the circles L meet tangentially. We explain in the Theory section how to derive appropriate boundary conditions where the spicules meet the sphere. Solving the axisymmetric Euler-Lagrange equations then determines a spicule shape, including an individual spicule volume V_s and area A_s. In terms of these variables, the overall area and volume of the RBC are taken to be

$$A \approx nA_s + 0.1 \times 4\pi R_0^2 \qquad (14)$$

and

$$V \approx \frac{4\pi}{3} R_0^3 + nV_s, \qquad (15)$$

with the spicule number

$$n_s \approx 3.6 \times \left(\frac{R_0}{r_L}\right)^2. \qquad (16)$$

In writing these relations, we have assumed that 10% of the spherical surface is not covered by the circular spicule bases (close packing on a flat surface would give 9.3%; curvature effects and packing defects both increase this number). The spicule volume V_s is calculated with respect to a plane through L, and Eq. 15 neglects curvature corrections. These approximations are good when the number of spicules is large, as it will turn out to be for the echinocyte shapes.

THEORY

Membrane mechanics

In our treatment, spicules are assumed to be axisymmetric, and individual spicules are joined to the central body along the contour L, as illustrated in Fig. 2. Thus, our calculation involves finding a family of energy-minimizing axisymmetric spicule shapes and selecting from that family those shapes consistent with appropriate mechanical boundary conditions applied along L.

Parametrization of the axisymmetric spicule shape is illustrated in Fig. 2. The variables z and r measure distances along and perpendicular to the symmetry axis, respectively, whereas s measures the arclength from the pole. The function $z(r)$ determines the shape. θ is the angle between the local normal and the symmetry axis; $C_m(r)$, $C_p(r)$ are the principal curvatures,

$$C_m = \frac{d\theta}{ds} \quad \text{and} \quad C_p = \frac{\sin \theta}{r}. \qquad (17)$$

In calculating the spicule shape, we shall assume that the relaxed cytoskeleton is locally flat, a good approximation as
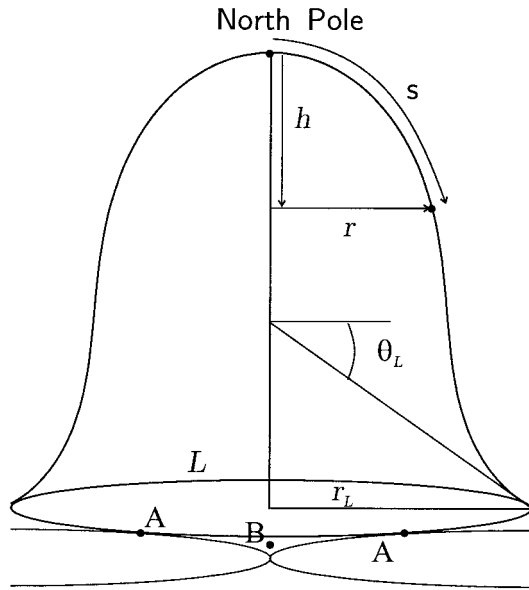
FIGURE 2 Parametrization of a single-spicule shape, showing the boundary L where the spicule joins the spherical central body in constructing the full echinocyte shape. The bases of two adjacent spicules are sketched in to illustrate the points A of spicule tangency and the point B, which is symmetrically situated between three neighboring spicules.

long as the number of spicules is large, so that the spicule size is small compared with R_0. Thus, in forming each spicule, a flat circular patch of relaxed cytoskeleton must be elastically deformed to fit the spicule contour. We assume that this deformation is axisymmetric, so that the center of the patch remains at the apex of the spicule, and each point of the patch at relaxed radius s_0 maps to a point at arclength s and radius r on the spicule contour. The principal extension ratios can then be written,

$$\lambda_1 = \frac{r}{s_0}, \quad \lambda_2 = \frac{ds}{ds_0}. \tag{18}$$

When these expressions for λ_1 and λ_2 are inserted into Eq. 4 we obtain an explicit form for the elastic energy in terms of the functions $s_0(s)$ and $r(s)$,

$$F_{el} = \pi K_\alpha \int s_0 ds_0 \left(\frac{r}{s_0} \frac{ds}{ds_0} - 1 \right)^2$$

$$+ \pi \mu \int s_0 ds_0 \left(\frac{r}{s_0} \frac{ds_0}{ds} + \frac{s_0}{r} \frac{ds}{ds_0} - 2 \right) \tag{19}$$

Using Eqs. 2, 3, 17, and 19, we can implement the stationarity condition for the free-energy functional (12) with respect to variations of membrane shape and cytoskeletal strain. This leads to a set of five coupled first-order differential equations, which are written down explicitly in the Appendix. Note that the ADE term in Eq. 3 enters only

through the appearance of an effective spontaneous curvature

$$C_0^{eff} = C_0 - \frac{\pi \alpha}{DA} (\Delta A - \Delta A_0), \tag{20}$$

which must be determined self-consistently via Eq. 5. Although these Euler-Lagrange equations look complicated, they can be related to simple mechanical force-balance conditions in a way that makes their content entirely transparent (Mukhopadhyay and Wortis, in preparation). We have used these equations to calculate (approximate) spicule shapes.

We now turn to the boundary condition where the spicules meet the sphere (see Fig. 2). Along each element of L, the spicule membrane exerts a tension $\tau_\parallel$ in the plane of the membrane and perpendicular to L, and a tension $\tau_\perp$ normal to the plane of the membrane. There is no tension in the third ("shear") direction because of the membrane fluidity. In addition, the membrane skeleton exerts an independent tension that must be in-plane, because the skeleton lacks bending rigidity. In general, these tensions would be different at different points of L; however, in the axisymmetric approximation, the tensions are uniform around L and the skeletal tension is directed radially. To maintain mechanical equilibrium, these tensions must balance where the spicules meet at point A. Note that A is a point of bilateral symmetry between the two adjacent spicules, so that in-plane tensions, which act in opposite directions, always balance by symmetry. On the other hand, the normal tensions $\tau_\perp$ must vanish individually, as they act in the same direction. The normal tension is related to the isotropic bending moment per unit length,

$$M = \kappa_b (C_p + C_m - C_0^{eff}), \tag{21}$$

by (Evans and Skalak, 1980; Mukhopadhyay and Wortis, in preparation) $\tau_\perp = dM/ds$. Thus, an appropriate boundary condition along L is

$$\frac{d(C_p + C_m)}{ds} = 0. \tag{22}$$

This is the boundary condition that we shall apply in our calculations. Of course, this boundary condition is approximate, because the real spicule is only approximately axisymmetric. Indeed, with equal logic, we could argue by symmetry that $\tau_\perp$ should vanish at point B, where three adjacent spicules meet at a radius from the spicule axis some 15% larger than r_L. We shall use this observation in the Results to get a rough measure of the error introduced by the approximation (22).

We now outline the algorithm used to solve numerically the Euler-Lagrange equations for stationary spiculated shapes. A "shooting method" was used to integrate the Euler-Lagrange equations from the apex to the edge of the spicule, the contour L along which the normal tension $\tau_\perp$

vanishes. The set of solutions can be characterized by five parameters. Three of them are the global parameters: the pressure difference P, the Lagrange multiplier Σ, and the effective spontaneous curvature C_0^{eff}, Eq. 20. The remaining two parameters correspond to initial values of variables in the integration procedure, i.e., the curvature ($C_m = C_p$) and the stretching ratios ($\lambda_1 = \lambda_2$) of the cytoskeleton at the pole. Integrating the Euler-Lagrange equations to a point where Eq. 22 is satisfied determines r_L and θ_L and, therefore, R_0 and n_s from Eqs. 13 and 16. The initial conditions may be adjusted iteratively to fit four parameters, A (Eq. 14), V (Eq. 15), $\overline{\Delta A_0}$ (Eq. 8), and the cytoskeletal stretching ratio, γ, which measures the ratio of the area of the calculated spicule to that of the corresponding relaxed cytoskeletal patch (roughly the same as the ratio of the area of the full echinocyte to that of the full relaxed membrane skeleton, as the corrections in Eq. 14 for the spherical segments are small). We are left, finally, with a one-parameter family of mechanical-equilibrium solutions, which we take to be labeled by the spicule number n_s. The predicted equilibrium configuration is the solution n_s^{eq}, which minimizes the overall energy. Of course, for the exact solution, n_s is a discrete variable. Probably, there exists, for given initial conditions, a set of distinct branches of solutions characterized by different values of n_s and different arrangements of spicules on the surface, as discussed more fully in the Discussion section.

Scaling analysis

Before proceeding to solutions, we wish to identify the important energy and length scales of the problem. Because we are working at a temperature that is effectively low, one overall energy scale drops out of the mechanical problem. We take this scale to be set by the bending modulus κ_b (κ_b and $\bar{\kappa}$ are similar in magnitude). There are three length scales. The first is the overall scale of the RBC, which we denote R. The second, we may take to be $1/\bar{C}_0$ from Eq. 7 (which is equivalent to using a length based on $\overline{\Delta A_0}$, Eq. 8); alternatively, we can take the second length to be $1/C_0^{\text{eff}}$, where C_0^{eff} is the effective spontaneous curvature from Eq. 20 (we assume that C_0 and C_0^{eff} are comparable in magnitude). The third length is the elastic length scale Λ_{el}, Eq. 1. In general, there may be other length scales associated with the relaxed cytoskeletal shape; however, we shall assume that any such lengths are comparable with R. For the RBC, $R \gg \Lambda_{\text{el}}$. The length scale $1/\bar{C}_0$ is a control parameter whose magnitude can be tuned across the range defined by R and Λ_{el}, resulting in the observed RBC shape classes.

The size of the RBC sets the total area and volume in the problem. Note that the RBC has a relatively smaller volume for a given surface area than a sphere. If a sphere with the same surface area has a volume V_{sphere}, then the ratio of RBC volume to that of the equivalent sphere defines a reduced volume, $v \equiv V_{\text{RBC}}/V_{\text{sphere}}$. For the RBC, $v \approx 0.6$,

significantly less than unity, which allows the RBC to assume its sequence of distinct nonspherical shapes. In its usual discocytic phase, the red blood cell is expected to have a magnitude of $1/\bar{C}_0$ that is of the order of the red blood cell dimensions or larger. Tuning $\bar{C}_0$ to sufficiently large positive values generates the sequence of evaginated echinocytic shapes; tuning it to sufficiently large negative values generates the sequence of invaginated stomatocytic shapes.

The significance of the elastic length scale Λ_{el} is that it determines how strong the effect of elasticity is for structures with some characteristic length, say L. To see this, we imagine rescaling the problem with the energy scale κ_b and the length scale L in such a way as to make all the parameters appearing in the Euler-Lagrange equations dimensionless. In this way, we arrive at the rescaled parameters,

$$\kappa_b' = 1$$

$$P' = PL^3/\kappa_b$$

$$\Sigma' = \Sigma L^2/\kappa_b$$

$$K_\alpha' = K_\alpha L^2/\kappa_b$$

$$\mu' = \mu L^2/\kappa_b$$

$$C_0^{\text{eff}'} = C_0^{\text{eff}}L. \tag{23}$$

Equivalent rescaling of the variables, $C_m' = C_mL$, etc., leaves the form of the Euler-Lagrange equations unchanged, although the parameter values (Eq. 23) vary with L. For example, suppose L is the echinocyte spicule radius. If $L > \Lambda_{\text{el}}$, then μ' is greater than unity, and the elastic terms from Eq. 2 dominate the bending-energy terms; conversely, if $L < \Lambda_{\text{el}}$, then μ' is smaller than one, and the bending-energy terms dominate. Thus, generically, elasticity is strong at length scales larger than Λ_{el} and weak at length scales smaller than Λ_{el}. This statement may seem surprising to those who think of the discocyte as effectively shaped by bending energy. The key point here is the plasticity of the membrane skeleton, albeit on time scales much longer than the induced shape changes we are discussing. If the relaxed membrane skeleton closely matches the shape preferred by bending energy alone, then (of course) elastic effects are small. This is apparently the case for the resting discocyte (but definitely not for the echinocyte).

A similar scaling argument gives insight into the characteristic spicule size in the echinocyte region. Suppose we let $L = \Lambda_{\text{el}}$ in Eq. 23. At this length scale, the bending and elastic terms (κ_b', K_α', and μ') are comparable and the only remaining parameters are P', Σ', and $C_0^{\text{eff}'}$ (or, equivalently, $\bar{C}_0'$). If, in addition, P' and Σ' are small, then the Euler-Lagrange equations are equivalent to those for the unconstrained minimization of the combined bending-plus-elastic problem (2). But, this is a problem that we understand.

When $C_0^{\mathrm{eff}'}$ is small in magnitude, then the membrane remains flat (at the length scale of Λ_{el}); on the other hand, when $C_0^{\mathrm{eff}'}$ is large in magnitude, then bending energy (which dominates the shape at scales below Λ_{el}) will favor budded shapes on the scale of $1/C_0^{\mathrm{eff}}$, either invaginated or evaginated depending on the sign of C_0^{eff}. Between these limits, when Λ_{el} and $1/C_0^{\mathrm{eff}}$ are comparable, we expect spicules (for positive C_0^{eff}) scaled by $1/C_0^{\mathrm{eff}}$, tending towards smoother shapes when Λ_{el} is somewhat smaller than $1/C_0^{\mathrm{eff}}$ and towards sharper, more columnar shapes when Λ_{el} is somewhat larger than $1/C_0^{\mathrm{eff}}$. Note that, as long as we rescale to the length Λ_{el}, the expected spicule shape is predicted to be independent of cell size R and to depend only on the scaled value of C_0^{eff} and the ratio of the two elastic constants, μ and K_α.

The above argument depends on the condition that the scaled values of P and Σ be small at the elastic length scale. For smooth and flaccid shapes like the discocyte (and when the cytoskeleton is not significantly stretched or compressed) the pressure difference P is generated by the bending energy, so P' is of order unity on the scale of the cell size R, and similarly for Σ'. It then follows from Eq. 23 that the condition is well satisfied for the discocyte and other nearby shapes (as we shall see, the initial echinocyte shapes fall into this class). Of course, if the system is pushed too hard, then this condition breaks down and other length scales enter the spicule-shape problem.

In summary, the shape of a spicule arises as a result of the interplay between the two length scales, Λ_{el} and $1/C_0^{\mathrm{eff}}$. When $1/C_0^{\mathrm{eff}}$ is positive and much larger than Λ_{el}, the effect of elasticity is strong and we can expect spicules that are at most gentle bumps. It is only when $1/C_0^{\mathrm{eff}}$ becomes of the order Λ_{el} or smaller that we may expect sharp spicules. Thus, if we look at the series of shape transformations, from discocytes through discocytes with gentle bumps to sharply spiculated structures, the sharp spicules will first arise with a radius comparable with Λ_{el}. We shall verify this scenario in the next section by explicit solution for the stable shapes.

RESULTS

In this section we report echinocyte shapes calculated according to the program outlined in the Theory section and using the elastic moduli (κ_b, $\bar{\kappa}$, μ, and K_α) given in Introduction and the RBC parameters (A and V) given in the Model section. The cytoskeletal stretching ratio γ is not known to good accuracy for the RBC. In this section, we take $\gamma = 1$; however, we have tested values in the range 0.7 to 1.2, and it is one of our results that variation within this range produces no appreciable changes in the number of spicules or their shape. The spontaneous curvature and relaxed area difference are not known and presumably vary somewhat over a typical RBC population; however, they enter the mechanics problem only in the combination $\overline{\Delta a}_0$, Eq. 9, which we take as our principal control parameter.
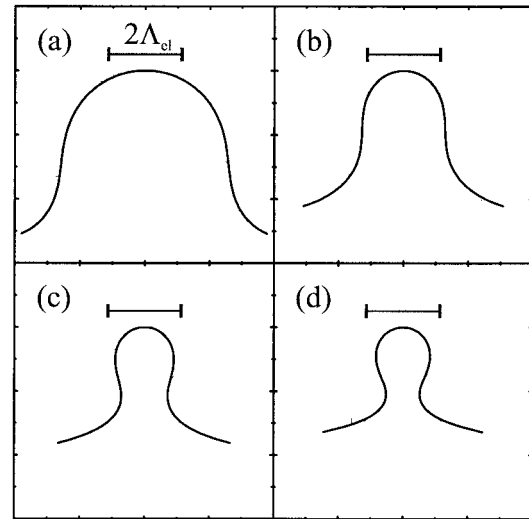
FIGURE 3 Sequence of spicule shapes for increasing values of the reduced effective relaxed area difference $\overline{\Delta a}\Delta a_0$, Eq. 9, which measures the combined effect of spontaneous curvature and additional area in the outer leaflet in driving the membrane to bend outward. (a–d) Correspond to $\overline{\Delta a}_0 = 0.014$, 0.018, 0.020, and 0.022, respectively. Note the bar shows the elastic length scale Λ_{el}. Note how the spicule sharpens as $\overline{\Delta a}_0$ increases and how the neck begins to form when the spicule dimension (set by $1/C_0^{\mathrm{eff}}$) falls below Λ_{el} so that the bending energy begins to dominate.

Fig. 3 displays the equilibrium spicule shapes that we obtain for a sequence of values of $\overline{\Delta a}_0$. Figs. 4 and 5 plot the corresponding calculated number of spicules n_s, which appear on the fully developed echinocyte III at equilibrium and the corresponding values of C_0^{eff} as functions of $\overline{\Delta a}_0$.

How well do the calculated shapes and spicule dimensions agree with experimental observations (Bessis, 1973;
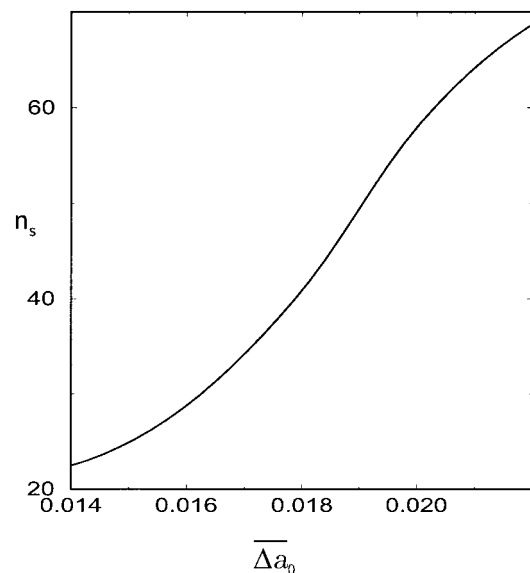

FIGURE 4 Calculated equilibrium number of spicules n_s plotted as a function of the reduced effective relaxed area difference $\overline{\Delta a}_0$.
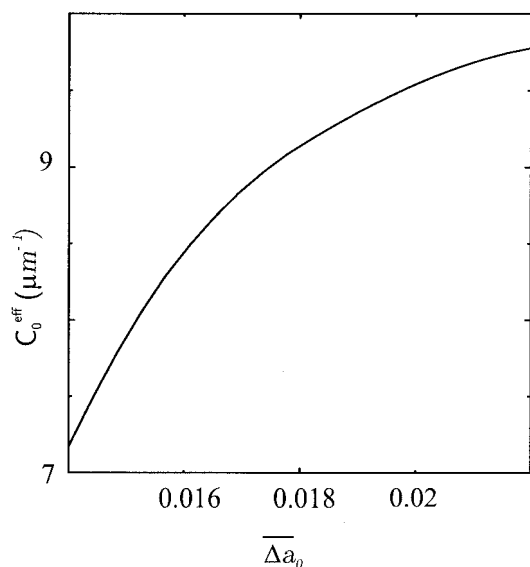
FIGURE 5 Calculated effective spontaneous curvature C_0^{eff}, Eq. 20, plotted as a function of $\overline{\Delta a}_0$.

Brecher and Bessis, 1972; Chailley et al., 1973). As shown in Fig. 3, the calculated shapes fall into three distinct categories. For n_s less than ~20, corresponding to $\overline{\Delta a}_0$ appreciably smaller than 0.016, the spicule shapes are broad and rather hat shaped, rather different from those seen in experiment. As $\overline{\Delta a}_0$ and C_0^{eff} increase, the number of spicules increases and the individual spicules become smaller, just as predicted by the scaling argument at the end of the previous section. By the time $\overline{\Delta a}_0$ is at or above 0.016, for n_s in the range 30–60, the spicule shapes are columnar with rounded tops, in good general agreement with the kinds of shapes seen in experiment. Beyond $n_s = 70$, the spicules become narrow-necked, a shape not typically seen in experiment but illustrating the dominance of the bending energy, as discussed in the Theory section.

In the "good," central region, the spicule dimensions and numbers are very comparable with those seen in experiment. A typical example ($\overline{\Delta a}_0 = 0.018$) is shown in Fig. 6 a.
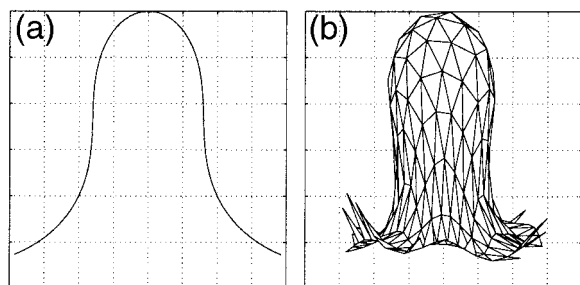

FIGURE 6 Calculated spicules at $\overline{\Delta a}_0 = 0.018$. (a) Shape found in the axisymmetric approximation, as discussed in this paper ($n_s = 41$, $R_0 = 2.57$ μm). (b) Shape found by numerical minimization on a triangulated surface ($n_s = 34$, $R_0 = 2.5$ μm).

For this case, we find $n_s = 41$, a radius of the central, spherical body of $R_0 = 2.57$, and an aspect ratio, height over width at base (which also corresponds approximately to the distance between adjacent spicules), of ~0.8, all of which are in reasonable agreement with observation. The only significant discrepancy is that the spicule height is close to 1.0 μm, somewhat larger than the range 0.6 to 0.8 μm seen in experiment, as is the aspect ratio. We shall comment on possible reasons for this discrepancy in the Discussion section. We emphasize that these shapes are a prediction of the model, not an assumption as they are in other recent work (Iglič, 1997; Iglič et al., 1998a,b). The only other spicule-shape predictions are those given by Waugh (1996), whose calculation suggests cross-sections that are less steep at the sides and more pointed at the apex than what is observed. Whether this is a consequence of the variational form assumed or of the neglect of stretching elasticity in the model is not clear. The calculations of Iglič et al., based on a postulated spicule shape and assuming skeletal incompressibility ($K_\alpha \to \infty$), produce somewhat higher values of the aspect ratio. At a given reduced area difference $\overline{\Delta a}_0$, they find a spicule number, which is larger than ours by almost a factor of two. We will return to some of these issues in the Discussion section.

Before discussing further what we shall argue are the nonbiological regions of hat-like and narrow-necked shapes, we must review the full echinocyte sequence (Brecher and Bessis, 1972; Bessis, 1973; Chailley et al., 1973; Mohandas and Feo, 1975). Experimental observations of RBCs, which are initially smooth, axisymmetric discocytes show that echinocytosis occurs in three stages. The first stage (echinocyte I) corresponds to irregular disc-like shapes with a central dimple. In the second stage (echinocyte II) the irregularities evolve into more or less well-defined spicules and the central dimple disappears, resulting in an oblately elliptical body decorated with spicules. In the third stage (echinocyte III) the central body becomes approximately spherical and the spicules become somewhat smaller and more numerous. When pushed beyond the echinocyte III, some kind of disconnection between the plasma membrane and the membrane skeleton occurs (see below) and plasma membrane is shed from the spicule tips into microscopic exovesicles. The remaining spherical shape with pointed protuberances is called a spheroechinocyte (Bessis, 1973).

Our calculation explicitly assumes that the central body is spherical and is, therefore, appropriate only for the late stage-III echinocyte. What we believe happens is that, for $\overline{\Delta a}_0 \lesssim 0.016$, the branch of echinocyte III shapes becomes energetically unstable to a branch of echinocyte II shapes. There is no internal way that our calculation can show that this crossover takes place; however, there are two pieces of evidence we find convincing. The first is a simple estimate. A separate calculation of the discocyte branch shows that its shape (and ΔA, for example) is roughly independent of $\overline{\Delta a}_0$,

allowing us to estimate its energy as a function of Δa_0. The calculated energy of our echinocyte III branch is lower than the discocyte branch but increases as $\overline{\Delta a_0}$ decreases. The crossing point of these two branches at $\overline{\Delta a_0} \sim 0.016$ is, thus, an approximate lower limit to the transition out of the echinocyte III phase. The actual transition out of the echinocyte III branch must presumably take place at a somewhat higher value of $\overline{\Delta a_0}$. The second piece of evidence is that, in separate work, which we shall report elsewhere (Lim, Wortis, Boal, and Mukhopadhyay, in preparation), we have done numerical simulations of RBC shapes using the same set of numerical parameters chosen here, and we find just such a transition at $\overline{\Delta a_0} \lesssim 0.017$ from the echinocyte III to a branch of echinocyte II shapes.

At the opposite end of the range of "good" spicule shapes, our calculation fails again and, again, for reasons that cannot be assessed internally. Here the size of the predicted spicule (set by the scale of $1/C_0^{eff}$) becomes comparable with the length of the elementary spectrin tetramer of the membrane skeleton (Liu et al., 1987). At this length scale, the continuum picture breaks down for the membrane skeleton (although it remains valid for the lipid component). What presumably happens is that a point of instability is reached, where lipid flow occurs and the plasma membrane buds outward in regions between the cytoskeletal anchors. Such buds, lacking cytoskeletal support, are known to be fragile. They presumably break off, leading to microvesiculation, membrane loss, and the observed spheroechinocytosis. Naturally, this vesiculation is expected to happen first at the spicule tips, where the elastic network is maximally expanded and the distance between anchors is largest.

In nature, the plasma membrane and its cytoskeleton are bound together by protein anchors; in our model this binding is replaced by the condition that the bilayer and the elastic network co-exist on the same mathematical surface. This requirement means that there is a local force per unit area or pressure Q with which the skeleton pulls inward ($Q > 0$) or pushes outward ($Q < 0$) on the membrane surface (or, equivalently, with which the membrane pulls outward or pushes inward, respectively, on the skeleton). The expression for this pressure is (Mukhopadhyay and Wortis, in preparation)

$$Q = C_m \left[K_\alpha \left(\frac{r}{s} \frac{dr}{ds} - 1 \right) + \frac{\mu}{2} \left(\left(\frac{s}{r} \right)^2 - \left(\frac{ds}{dr} \right)^2 \right) \right]$$

$$+ C_p \left[K_\alpha \left(\frac{r}{s} \frac{dr}{ds} - 1 \right) - \frac{\mu}{2} \left(\left(\frac{s}{r} \right)^2 - \left(\frac{ds}{dr} \right)^2 \right) \right] \quad (24)$$

and it is plotted in Fig. 7 as a function of the radial distance r from the spicule axis for $\overline{\Delta a_0} = 0.018$. As expected, Q is positive close to the tip of the spicule and negative around the neck where the skeleton has been compressed. The magnitude of the pressure at the spicule tip is of the order of 20 pN/μm^2. It is useful to compare this pressure to the
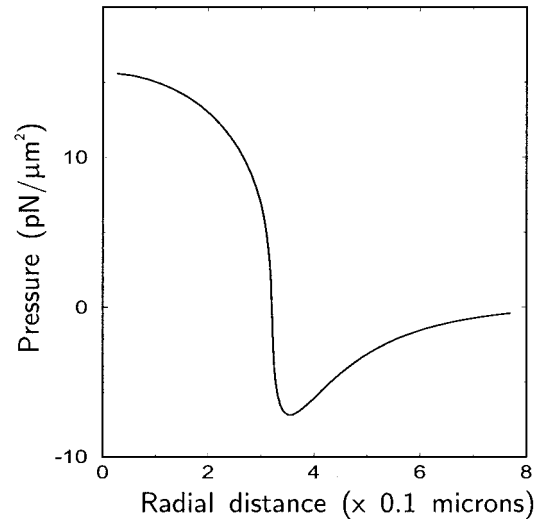

FIGURE 7   The local pressure Q, Eq. 24, exerted by the cytoskeleton on the bilayer plotted as a function of radial distance, for a spicule corresponding to $\overline{\Delta a_0} = 0.020$.

critical disjoining pressure necessary to break the anchoring and to separate the membrane skeleton from the bilayer. This critical pressure has not, to the best of our knowledge, been measured; nevertheless, it can be estimated. We take 10 pN as a crude estimate of the force required to extract quickly a single anchoring protein from the bilayer. Taking into account the density of anchors, we estimate a detachment pressure of $\sim$2000 pN/μm^2 (consistent with measurements reported in Waugh and Bausserman, 1995), two orders of magnitude larger than what we have calculated above. This comparison is important, as membrane-cytoskeleton disjoining is another potential mechanism for spheroechinocytosis, an alternative to the one discussed in the paragraph above and has, indeed, been proposed by Iglič and others (Iglič et al., 1995, 1996). We conclude that such direct disjoining seems unlikely, unless it is associated with anchoring defects.

We have seen for the human erythrocyte that the fully developed echinocyte III, with well developed spicules, first appears when $1/C_0^{eff}$ becomes small enough to be comparable with the elastic length scale Λ_{el}. It is a plausible hypothesis that this is a general connection. If so, there is a direct relation between the spicule dimension at the onset of the echinocyte III and the ratio (Eq. 1) of the bending rigidity to the elastic moduli. Interestingly, Smith et al. (1982) have studied spiculated shapes for the red cells of a variety of species. Despite considerable variation in the volume of the red cells (ranging from the goat RBC, which is appreciably smaller than the human one, through the elephant seal, which is appreciably larger) the spicule size is quite stable, suggesting that the elastic length scale is not strongly variable from one species to another. This means, of course, that the number of spicules on the typical echi-
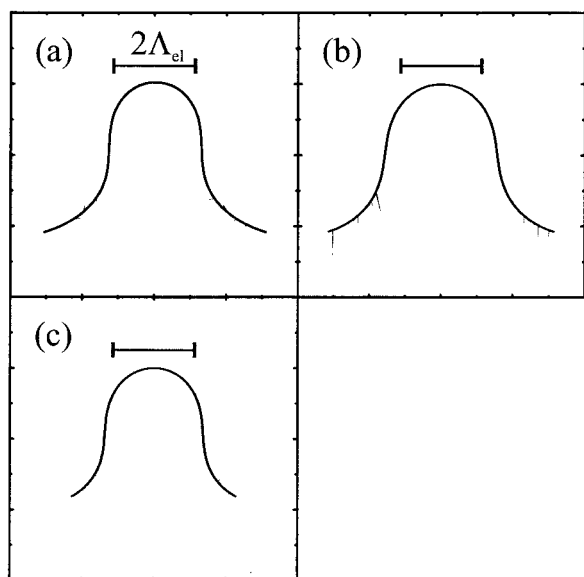
FIGURE 8 Dependence of spicule shape on parameters at $\overline{\Delta a}_0 = 0.018$. (*a*) Shape with the standard RBC parameters, as discussed in the text. (*b*) Effect of starting from *a* and increasing K_α by a factor of 2 (i.e., $K_\alpha = 6$ μ). The spicules become slightly broader. (*c*) Effect of reducing overall cell dimension by a factor of two, so that $V \rightarrow V/8$ and $A \rightarrow A/4$. This change reduces spicule size by $\sim 10\%$.

nocyte is small for the goat (~ 10) and large for the elephant seal (~ 100), as observed. To illustrate this point further, we plot in Fig. 8 spicule shapes at different volumes and different ratios K_α/μ but with Λ_{el} held fixed. We find that at smaller volume, the spicules sizes do become smaller but the dependence on volume is weak. The dependence on the ratio of elastic constants K_α/μ is even weaker. At a value of K_α that is larger by a factor of 2 ($K_\alpha = 6$ μ), the spicules become somewhat broader and their number decreases by $\sim 5\%$. Of course, the local stretching of the cytoskeleton both at the spicule apex and in the neck region close to the base may be expected to change considerably.

These results are based on the model described in the Theory section, which assumes spicule axisymmetry, as incorporated in the (approximate) boundary condition, Eq. 22. In closing this section, it may be useful to comment on the reliability of this central assumption. We have two remarks. The first concerns the boundary condition. The neighborhood of a given spicule is clearly not axially symmetric, so this condition is clearly approximate. If the calculated shapes depended sensitively on the precise way that this boundary condition is applied, then results based upon it would be suspect. We motivated the boundary condition ($\tau_\perp = 0$) by looking at the point labeled A in Fig. 2, where adjacent spicules are tangent. With equal logic, we could have argued this boundary condition at the point labeled B. If we made this choice, how different would the calculated spicule shapes turn out to be? We have run some test cases and find changes in, e.g., the spicule height of less than 1%,

suggesting that the results are strongly insensitive to the details of the boundary condition. But, this is far from sufficient. As a second test, we have recently completed a program (Lim, Wortis, Boal, and Mukhopadhyay, in preparation) of direct simulation of the energy functional (2) on a triangulated surface. This program allows us to calculate echinocyte shapes without assumptions about spicule axisymmetry. We find echinocyte shapes in this region of parameter space and can compare the simulated spicule shapes with those calculated here at the same parameter values. Fig. 6 shows one such comparison. Although the base of the simulated spicule is a little narrower than that given by the approximate axisymmetric calculation, the overall level of agreement is excellent. At these parameter values, the number of spicules in our calculation is 41, whereas the number found by simulation is 34. Similarly, the radius of the central spherical body to which our spicules are fitted is 2.57 μm, whereas that found in the simulations is ~ 2.5 μm (the central body is only roughly spherical in this case). The approximate calculation presented in this paper appears to be reasonably reliable.

DISCUSSION

The calculations presented here build on the previous work of Iglič et al. (1998a,b; Iglič, 1997) and show that a simple mechanical model of a uniform composite membrane can give a good account of observed echinocyte shapes. The central control parameter in this process is the effective area difference (or curvature) of the lipid component, in agreement with the bilayer-couple hypothesis of Sheetz and Singer (1974). The role of the cytoskeletal elasticity is to suppress the formation of narrow-necked buds, which would form in the absence of cytoskeletal shear resistance. Does this good agreement prove that mechanics (as opposed to biochemistry) is the sole determinant of echinocyte shape? It does not. However, it does strongly suggest that simple mechanics will play an important role in any complete picture. We end this section with a brief discussion of some loose ends and future directions.

Elastic constants and elastic nonlinearities

There has been much discussion in the literature of what are the "correct" elastic constants to use for the membrane skeleton. We have chosen $\mu \approx 2.5 \times 10^{-6}$ J/m^2 and $K_\alpha \approx 3$ μ. These values are in rough agreement with recent measurements at low deformation (Hénon et al., 1999; Lenormand et al., 2001) and somewhat lower than those reported in connection with pipette aspiration of red cells (Evans, 1973a,b; Waugh and Evans, 1979) where large deformations play an important role.

Discussion of values of the elastic moduli is complicated by the occurrence of nonlinearities in the elastic response.

At low deformation, $\lambda_i = 1 + \epsilon_i$ with ϵ_i small, there are only two rotational invariants from which to construct the elastic energy, $\frac{1}{2}(\epsilon_1 + \epsilon_2)^2$ and $\frac{1}{2}(\epsilon_1 - \epsilon_2)^2$, whose coefficients define the linear moduli of stretching and shear elasticity. It is easy to verify that these linear moduli are just K_α and μ, respectively. However, at large deformation, terms of higher orders in $(\epsilon_1 + \epsilon_2)$ and $(\epsilon_1 - \epsilon_2)^2$ will generally also appear in the elastic energy, each with its own coefficient. The expression (4) for the elastic energy makes a particular choice for each of these coefficients, one which is simply proportional to the linear moduli. At small extension ratios, these higher-order terms are unimportant; however, for the echinocyte shapes, we find ϵ_i of order unity, so these terms cannot be neglected. Unfortunately, present experiments do not constrain the values of the higher order coefficients significantly, although it is probably not an accident that the moduli derived from the pipette aspiration experiments (Evans, 1973a,b), which have extension ratios up to nearly 2 (Lee et al., 1999), are larger than those measured in the linear regime (Henon et al., 1999; Lenormand et al., 2001). This suggests a hardening of the elasticity at large deformation, consistent, for example, with terms in $(\epsilon_1 + \epsilon_2)^3$, $(\epsilon_1 + \epsilon_2)(\epsilon_1 - \epsilon_2)^2$, and so forth, coming into play. We will deal with the issue of nonlinearity at more length in a future publication. For the present, we simply remark that realistic spicule formation does require a proper balance between stretching and shear energies at large deformation. Our chosen ratio of $K_\alpha/\mu = 3$ suffices; however, a lower ratio plus some additional nonlinear hardening would also achieve the same effect and may be more realistic. Any effect that changes spicule shape significantly may also be expected to modify quantitatively the regions of stability of different shape classes.

Previous variational work on echinocyte shapes by Iglič and coworkers (Iglič, 1997; Iglič et al., 1998a,b) has assumed local incompressibility of the cytoskeleton ($K_\alpha \to \infty$), thus forcing all the elastic energy into the shear term. This was done for practical reasons; we are now in a position to understand the effect of this approximation. Fig. 8 c suggests that increasing K_α at fixed μ has a modest effect on spicule shape, decreasing the height and the base radius somewhat without changing the mean radius appreciably. This is consistent with the generally larger number of spicules predicted by Iglič et al. (1998a,b; Iglič, 1997). Because of the limited shapes available in the variational parametrization, these authors cannot follow the full spicule-shape evolution exhibited in our Fig. 3.

Spicule placement, metastability, and related matters

Our calculation assumes for the echinocyte regular spicule placement with sixfold coordination on a central spherical body. Of course, this is only an approximation. First, there is the topological requirement for a net undercoordination of

12. More generally, if the energy minimization problem were to be solved exactly, we would expect to find several distinct sheets of locally minimizing shapes with different spicule numbers n_s and different spicule organization. For any given set of parameter values, one such shape would have the lowest energy; however, several others might have nearby energies. Metastability of a shape would be expected, because the energy landscape is on the scale of κ_b, which is large on the scale of $k_B T_{room}$. This metastability, in turn, would cause hysteresis in the shape transformations.

Some experiments show that, as the red cell is chemically cycled back and forth between discocyte and echinocyte phases, spicules always appear at the same locations on the cell surface (Furchgott, 1940; Bessis and Prenant, 1972), suggesting that spicule placement could be intrinsically related to defects and other inhomogeneities in the cytoskeleton. This would not happen in a continuum model. Without wishing to dispute the experimental evidence, we can only say that our work shows that spicule formation does not require cytoskeletal inhomogeneity. Of course, if inhomogeneities exist, then they will have an effect in selecting the pattern of spicule placement.

It is not clear a priori whether or not the spicule is a solitonic object with its own intrinsic scale and, if so, whether spicules tend to attract or repel at long distance. Some recent work (Lim, Wortis, Boal, and Mukhopadhyay, in preparation) has suggested long-range attraction, which would mean that, under appropriate circumstances, spicule clumping might occur, leaving "bald" regions on the echinocyte surface, as is seen in some pictures of echinocyte shapes (see, for example, Iglič et al., 1998a). None of this finer detail is captured in our approximation.

Extended shape/phase diagram

We have focussed on the spontaneous curvature or area difference $\overline{\Delta a_0}$ as the principal parameter controlling the evolution of echinocyte shape. Of course, induced changes in any parameter of the membrane energy expression Eqs. 2 to 4 and the constraints V and A, singly or in combination, will affect the cell shape. A (bio)chemical modification of the red-cell environment presumably changes all these parameters to some extent; it is just that some changes are larger and more important than others. If there are situations in which laboratory reagents cause important modification in other parameters (e.g., the elastic constants) then addition of these reagents will cause the red cell to be driven along a trajectory in an extended parameter space. In such a situation, we would need to consider the minimum-energy shape (or shapes) as functions of several variables in an extended shape/phase diagram. The work surrounding Fig. 8 illustrates the beginning of such a study.

We have summarized in the Introduction the mechanism by which some common reagents affect the Sheetz-Singer (1974) parameter $\overline{\Delta a_0}$. The pH effect and the associated

glass effect are less readily related to $\overline{\Delta a_0}$ but may well be primarily related to another dimension of the generalized phase diagram. For example, Gedde et al. (1995) have shown that lipid asymmetry and the presence of inner leaflet titratable groups, which might be expected to be associated with $\overline{\Delta a_0}$, do not have appreciable influence on the pH effect; however, Elgsaeter et al. (1986) and Stokke et al. (1986) have shown that the membrane skeleton expands in vitro in response to high cytoplasmic pH. Now, according to the scaling argument (Eq. 11), we know that such expansion is equivalent to decreasing the shear modulus μ and, therefore, to increasing the elastic length scale Λ_{el} (1). But, echinocytosis occurs when $1/C_0^{\text{eff}}$ shrinks below Λ_{el}. Thus, at fixed C_0^{eff} (roughly equivalent to fixed $\overline{\Delta a_0}$), expanding the membrane skeleton could promote echinocytosis, as observed. It would be premature to claim that this is the full explanation of the pH effect. The point is that, as long as changes in biochemical variables produce homogeneous changes in the material parameters that appear in Eqs. 2 through 4, our model continues to apply, although the relevant experimental trajectories may be in a larger parameter space.

Membrane composition, inhomogeneity, and charge effects

Description of any effects that lead to inhomogeneity in membrane properties requires modification of our model. One such effect that is certainly present arises from the inhomogeneous distribution of lipids and/or proteins. We know that the plasma membrane is composed of a mixture of lipids and proteins. The bending modulus κ_{b} depends on membrane composition. As long as the composition remains homogeneous, the model Eqs. 2 to 4 holds; but, any mechanism that produces compositional inhomogeneity on the scale of RBC shape features would necessitate modification of the model. Thus, for example, observed raft formation (Simons and Toomre, 2000; Pralle et al., 2000) suggests membrane inhomogeneity on the scale of 0.05 to 0.07 μm. When local radii of curvature become comparable with the inhomogeneity scale, then inhomogeneity is expected to influence shape. This may occur for the echinocyte near the spheroechinocyte limit; however, there is no evidence that it is a dominant effect elsewhere.

Other interesting effects involve the coupling of lipid composition to geometry. Thus, for example, outer-leaflet lipids with large heads may be expected to segregate preferentially to spicule tips as would inner-leaflet lipids with large tails. Such an effect could be included in a mechanical model by adding a composition field (or fields) and including terms coupling composition to curvature. Alternatively, one might imagine mechanisms involving membrane components that preferentially favor (or avoid) regions around the cytoskeletal anchoring complexes. These components would be relatively dilute (concentrated) in regions where the cytoskeleton was significantly expanded (as it is near the spicule tip). To represent this effect, one would need to couple composition to local cytoskeletal strain.

Whereas these mechanisms may be present to some extent in the red cell, our calculations suggest they are not in any way required for spicule formation.

Finally, chemical groups that carry net charge at physiological pH are common both for lipid headgroups and for cytoskeletal components. As long as these charges are compensated by counterions on scales smaller than the local radii of curvature, they enter the mechanics only via their effect on the mechanical moduli. On the other hand, when relevant lengths become comparable with or smaller than the Debye length, then charge effects must be treated as nonlocal.

Conclusions

Our calculation provides echinocyte sizes and shapes in excellent agreement with experiment. Although shapes are calculated under the approximation of spicule axisymmetry, there is evidence (e.g., Fig. 6) that this approximation is good. The approximation does not allow us to estimate internally the range of echinocyte III stability; however, extrinsic arguments (see Results) suggest that observable shapes should be bounded at low $\overline{\Delta a_0}$ in the region where $1/C_0^{\text{eff}}$ first becomes smaller than Λ_{el} and at large $\overline{\Delta a_0}$ in the region where the spicule dimension becomes comparable with the cytoskeletal discreteness. And, indeed, outside this region the predicted shapes are no longer seen experimentally. Whereas this consistency lends credibility to the continuum picture, the way in which biochemical influences drive the control parameters of the model is not addressed. The Sheetz-Singer parameter, $\overline{\Delta a_0}$, which measures the area difference between the lipid monolayers (and the related effect of membrane spontaneous curvature) does seem to be the dominant control parameter for some kinds of induced shape change. On the other hand, other effects (such as the pH effect) may probe other dimensions of the shape/phase diagram, e.g., the role of the cytoskeletal elastic constants and prestress. We hope that having a mechanical model with predictive power may eventually help to elucidate important biochemical questions. From this perspective, experiments can now focus on the way in which biochemical probes affect all the mechanical control parameters, including elastic and cytoskeletal variables, in addition to $\overline{\Delta a_0}$.

APPENDIX A

Euler-Lagrange Equations

In this Appendix we demonstrate how the Euler-Lagrange equations for the membrane arise from the constrained minimization of the free energy Eqs. 2 to 4. For simplicity, we shall omit the second (ADE) term in Eq. 3. The effect of including this term is simply to convert the spontaneous curvature C_0 into the effective spontaneous curvature $\overline{C}_0$ defined by Eq. 7. Following

Peterson (1985), we use the arc length s as the parametrization variable and compose the free-energy functional,

$$\Psi[\sigma, P, b(s)] = F + \sigma A - PV$$

$$+ \pi \int_0^{s^\star} ds\, b(s)\left[\frac{dr}{ds} - \cos\theta\right]$$

$$= \pi \int_0^{s^\star} ds\, \mathcal{L}(s, s_0, r, \theta, b)$$

$$= \pi \int ds\left\{ s_0\frac{ds_0}{ds}\left[K_\alpha\left(\frac{r}{s_0}\frac{ds}{ds_0} - 1\right)^2 \right.\right.$$

$$\left.+ \mu\left(\frac{r}{s_0}\frac{ds_0}{ds} + \frac{s_0}{r}\frac{ds}{ds_0} - 2\right)\right]$$

$$+ r\kappa_b\left(\frac{d\theta}{ds} + \frac{\sin\theta}{r} - C_0\right)^2$$

$$+ 2\sigma r - Pr^2\cos\theta$$

$$\left.+ b(s)\left[\frac{dr}{ds} - \cos\theta\right]\right\}, \quad (A1)$$

in which $s^\star$ is the overall arc length and the last term was introduced to impose the local constraint $dr/ds = \cos\theta$. The function $b(s)$ is a "Lagrange-multiplier function," which enforces this constraint. We now treat the variables s_0, r, θ, and b as independent functions of the arc length s. Making the free-energy functional (Eq. A1) stationary against arbitrary variations of b, θ, and r leads, respectively, to the equations,

$$\frac{dr}{ds} = \cos\theta \quad (A2)$$

$$\frac{dC_m}{ds} = \frac{\cos\theta\sin\theta}{r} - \frac{C_m\cos\theta}{r} - \frac{Pr\cos\theta}{2\kappa_b} + \frac{b\sin\theta}{2r\kappa_b}$$

$$\quad (A3)$$

$$\frac{db}{ds} = 2K_\alpha\left(\frac{ds}{ds_0}\frac{r}{s_0} - 1\right) + \mu s_0\frac{ds_0}{ds}\left(\frac{1}{s_0}\frac{ds_0}{ds} - \frac{s}{r^2}\frac{ds}{ds_0}\right)$$

$$+ (2\sigma + \kappa_b C_0^2) + \kappa_b[C_m^2 - 2C_0 C_m - C_p^2]$$

$$- 2Pr\sin\theta, \quad (A4)$$

in which $C_m \equiv d\theta/ds$. In addition, because the integrand $\mathcal{L}$ in Eq. A1 has no explicit dependence on s, the "Hamiltonian function,"

$$\mathcal{H}(s) \equiv \dot{s}_0\frac{d\mathcal{L}}{d\dot{s}_0} + \dot{r}\frac{d\mathcal{L}}{d\dot{r}} + \dot{\theta}\frac{d\mathcal{L}}{d\dot{\theta}} - \mathcal{L}, \quad (A5)$$

(in which, for example, $\dot{s}_0 \equiv ds_0/ds$) is conserved, i.e., independent of s. It is easy to show that, for the variables to be well behaved close to the north

pole ($s = 0$), in which $r = 0$, $\mathcal{H}$ has to vanish at $s = 0$, implying that $\mathcal{H}$ is identically zero along the entire shape contour. Therefore,

$$2K_\alpha r\left(\frac{ds}{ds_0}\frac{r}{s_0} - 1\right) + \mu s_0\left(\frac{s_0}{r} - \frac{r}{s_0}\left(\frac{ds_0}{ds}\right)^2\right)$$

$$+ r(2\sigma + \kappa_b C_0^2) + \kappa_b r[C_p^2 - 2C_0 C_p - C_m^2]$$

$$- b(s)\cos\theta - Pr^2\sin\theta \equiv -\mathcal{H} = 0. \quad (A6)$$

Making Eq. A1 stationary with respect to variations of s_0 leads to an equation equivalent to the derivative of Eq. A6 with respect to s and is not an independent condition.

Eqs. A2 through A4 plus Eq. A6 constitute the full set of Euler-Lagrange equations. The surface tension σ in these equations is, in general, shifted from the parameter Σ appearing in Eq. 12. If K_α and μ are set to zero in these equations, the well-known Euler-Lagrange equations for axisymmetric shapes of bilayer vesicles with no cytoskeleton reemerge. A final technical point is axisymmetric vesicle forms such as cylinders, which do not close smoothly at the poles are described by the same equations only with a value of the conserved Hamiltonian $\mathcal{H}$, which is consistent with the boundary conditions and does not generally vanish.

REFERENCES

Alberts, B., D. Bray, J. Lewis, M. Raff, K. Roberts, and J. D. Watson. 1994. Molecular Biology of the Cell, 3rd ed., Chapts. 10 and 16. Garland Publishing, New York.

Backman, L. 1986. Shape control in the human red cell. *J. Cell Sci.* 80:281–298.

Bennett, V. 1990. Spectrin-based membrane skeleton: a multipotential adaptor between plasma membrane and cytoplasm. *Physiol. Rev.* 70: 1029–1065.

Bessis, M. 1973. Living Blood Cells and Their Ultrastructure. R. I. Weed, editor. Springer-Verlag, New York.

Bessis, M., and M. Prenant. 1972. Topographie de l'apparition des spicules dans les érythrocytes crénelés (échinocytes). *Nouv. Rev. Fr. Hémat.* 12:351–364.

Boal, D. H. 1994. Computer simulation of a model network for the erythrocyte cytoskeleton. *Biophys. J.* 67:521–529.

Božič, B., S. Svetina, B. Žekš, and R. E. Waugh. 1992. Role of lamellar membrane structure in tether formation from bilayer vesicles. *Biophys. J.* 61:963–973.

Brecher, G., and M. Bessis. 1972. Present status of spiculated red cells and their relationship to the discocyte-echinocyte transformation: a critical review. *Blood.* 40:333–344.

Byers, T. J., and D. Branton. 1985. Visualization of the protein associations in the erythrocyte membrane skeleton. *Proc. Natl. Acad. Sci. U.S.A.* 82:6153–6157.

Canham, P. B. 1970. The minimum energy of bending as a possible explanation of the biconcave shape of the human red blood cell. *J. Theor. Biol.* 26:61–81.

Chailley, B., R. I. Weed, P. F. Leblond, and J. Maigné. 1973. Formes échinocytaires et stomatocytaires du globule rouge. *Nouv. Rev. Fr. Hémat.* 13:71–87.

Christiansson, A., F. A. Kuypers, B. Roelofsen, J. A. F. Op Den Kamp, and L. L. M. Van Deenen. 1985. Lipid molecular shape effects erythrocyte morphology: a study involving replacement of native phosphatidylcholine with different species followed by treatment of cells with sphingomyelinase C or phospholipase A. *J. Cell Biol.* 101:1455–1462.

Deuling, H. J., and W. Helfrich. 1976. The curvature elasticity of fluid membranes: a catalogue of vesicle shapes. *J. Phys. (Paris).* 37:1335–1345.

Deuticke, B. 1968. Transformation and restoration of biconcave shape of human erythrocytes induced by amphiphilic agents and changes of ionic environment. *Biochim. Biophys. Acta.* 163:494–500.

Discher, D. E., N. Mohandas, and E. A. Evans. 1994. Molecular maps of red cell deformation: hidden elasticity and in situ connectivity. *Science.* 266:1032–1035.

Döbereiner, H.-G., E. Evans, M. Kraus, U. Seifert, and M. Wortis. 1997. Mapping vesicle shapes into the phase diagram: a comparison of theory and experiment. *Phys. Rev. E.* 55:4458–4474.

Elgsaeter, A., B. T. Stokke, A. Mikkelsen, and D. Branton. 1986. The molecular basis of erythrocyte shape. *Science.* 234:1217–1223.

Evans, E. A. 1973a. A new material concept for the red cell membrane. *Biophys. J.* 13:926–940.

Evans, E. A. 1973b. New membrane concept applied to the analysis of fluid shear- and micropipette-deformed red blood cells. *Biophys. J.* 13:941–954.

Evans, E. A. 1974. Bending resistance and chemically induced moments in membrane bilayers. *Biophys. J.* 14:923–931.

Evans, E. A., and R. Skalak. 1980. Mechanics and Thermodynamics of Biomembranes. CRC Press, Boca Raton, FL.

Ferrell, J. E. Jr., K. J. Lee, and W. H. Huestis. 1985. Membrane bilayer balance and erythrocyte shape: a quantitative assessment. *Biochemistry.* 24:2849–2857.

Fourcade, B., L. Miao, M. Rao, and M. Wortis. 1994. Scaling analysis of narrow necks in curvature models of fluid lipid-bilayer vesicles. *Phys. Rev. E.* 49:5276–5286.

Fung, Y. C., and P. Tong. 1968. Theory of the sphering of red blood cells. *Biophys. J.* 8:175–198.

Furchgott, R. F. 1940. Observation on the structure of red cell ghosts. *Cold Spring Harbor Symp. Quant. Biol.* 8:224–232.

Furchgott, R. F., and E. Ponder. 1940. Disk-sphere transformation in mammalian red cells: II. The nature of the anti-sphering factor. *J. Exp. Biol.* 17:117–127.

Gedde, M. M., D. K. Davis, and W. H. Huestis. 1997b. Cytoplasmic pH and human erythrocyte shape. *Biophys. J.* 72:1234–1246.

Gedde, M. M., and W. H. Huestis. 1997a. Membrane potential and human erythrocyte shape. *Biophys. J.* 72:1220–1233.

Gedde, M. M., E. Yang, and W. H. Huestis. 1995. Shape response of human erythrocytes to altered cell pH. *Blood.* 4:1595–1599.

Gedde, M. M., E. Yang, and W. H. Huestis. 1999. Resolution of the paradox of red cell shape changes in low and high pH. *Biochim. Biophys. Acta.* 1417:246–253.

Gennis, R. B. 1989. Biomembranes: Molecular Structure and Function, Chapter 4. Springer-Verlag, New York.

Gimsa, J. 1998. A possible molecular mechanism governing human erythrocyte shape. *Biophys. J.* 75:568–569.

Gimsa, J., and C. Ried. 1995. Do band 3 protein conformational changes mediate shape changes of human erythrocytes? *Mol. Membr. Biol.* 12:247–254.

Hägerstrand, H., M. Danieluk, M. Bobrowska-Hägerstrand, A. Iglič, A. Wróbel, B. Isomaa, and M. Nikinmaa. 2000. Influence of band 3 protein absence and skeletal structures on amphiphile- and Ca^{2+}-induced shape alterations in erythrocytes: a study with lamprey (*Lampetra fluviatilis*), trout (*Onochorhynchus mykiss*), and human erythrocytes. *Biochim. Biophys. Acta.* 1466:125–138.

Helfrich, W. 1973. Elastic properties of lipid bilayers: theory and possible experiments. *Z. Naturforsch.* C28:693–703.

Hénon, S., G. Lenormand, A. Richert, and F. Gallet. 1999. A new determination of the shear modulus of the human erythrocyte membrane using optical tweezers. *Biophys. J.* 76:1145–1151.

Iglič, A. 1997. A possible mechanism determining the stability of spiculated red blood cells. *J. Biomech.* 30:35–40.

Iglič, A., V. Kralj-Iglič, and H. Hägerstrand. 1998a. Stability of spiculated red blood cells induced by intercalation of amphiphiles in cell membrane. *Med. Biol. Eng. Comput.* 36:251–255.

Iglič, A., V. Kralj-Iglič, and H. Hägerstrand. 1998b. Amphiphile induced echinocyte-spheroechinocyte transformation of red blood cell shape. *Eur. Biophys. J.* 27:335–339.

Iglič, A., S. Svetina, and B. Žekš. 1995. Depletion of membrane skeleton in red blood cell vesicles. *Biophys. J.* 69:274–279.

Iglič, A., S. Svetina, and B. Žekš. 1996. A role of membrane skeleton in discontinuous red blood cell shape transformations. *Cell. Mol. Biol. Lett.* 1:137–144.

Isomaa, B., H. Hägerstrand, and G. Paatero. 1987. Shape transformations induced by amphiphiles in erythrocytes. *Biochim. Biophys. Acta.* 899: 93–103.

Jay, D. G. 1996. Role of band 3 in homeostasis and cell shape. *Cell.* 86:853–854.

Landman, K. A. 1984. A continuum model for a red blood cell transformation: sphere to crenated sphere. *J. Theor. Biol.* 106:329–351.

Lange, Y., A. Gough, and T. L. Steck. 1982. Role of the bilayer in the shape of the isolated erythrocyte membrane. *J. Membr. Biol.* 69: 113–123.

Lange, Y., and J. M. Slayton. 1982. Interaction of cholesterol and lysophosphatidylcholine in determining red cell shape. *J. Lipid Res.* 23: 1121–1127.

Lee, J. C., D. T. Wong, and D. E. Discher. 1999. Direct measures of large, anisotropic strains in deformation of the erythrocyte cytoskeleton. *Biophys. J.* 77:853–864.

Lenormand, G., S. Hénon, A. Richert, J. Siméon, and F. Gallet. 2001. Direct measurement of the area expansion and shear moduli of the human red blood cell membrane skeleton. *Biophys. J.* 81:43–56.

Liu, S. C., L. H. Derick, and J. Palek. 1987. Visualization of the hexagonal lattice in the erythrocyte membrane skeleton. *J. Cell Biol.* 104:527–536.

Low, P. S., B. M. Willardson, N. Mohandas, M. Rossi, and S. Shohet. 1991. Contribution of the band 3-ankyrin interaction to erythrocyte membrane mechanical stability. *Blood.* 77:1581–1586.

Miao, L., U. Seifert, M. Wortis, and H.-G. Döbereiner. 1994. Budding transitions of fluid-bilayer vesicles: the effect of area-difference elasticity. *Phys. Rev. E.* 49:5389–5407.

Mohandas, N., and C. Feo. 1975. A quantitative study of the red cell shape changes produced by anionic and cationic derivatives of phenothiazines. *Blood Cells.* 1:375–384.

Nakao, M., T. Nakao, and S. Yamazoe. 1960. Adenosine triphosphate and maintenance of shape of the human red cells. *Nature (Lond.).* 187: 945–946.

Nakao, M., T. Nakao, S. Yamazoe, and H. Yoshikawa. 1961. Adenosine triphosphate and shape of erythrocytes. *J. Biochem.* 49:487–492.

Nakao, K., T. Wada, T. Kamiyama, M. Nakao, and K. Nagano. 1962. A direct relationship between adenosine triphosphate-level and *in vivo* variability of erythrocytes. *Nature.* 194:877–878.

Peterson, M. A. 1985. An instability of the red blood cell shape. *J. Appl. Phys.* 57:1739–1742.

Ponder, E. 1948. Hemolysis and Related Phenomena. Grune and Stratton, New York.

Ponder, E. 1955. Red Cell Structure and Its Breakdown. Springer-Verlag, Vienna.

Pralle, A., P. Keller, E. L. Florin, K. Simons, and J. K. Horber. 2000. Sphingolipid-cholesterol rafts diffuse as small entities in the plasma membrane of mammalian cells. *J. Cell Biol.* 148:997–1008.

Schwarz, S., B. Deuticke, and C. W. Haest. 1999a. Passive transmembrane redistributions of phospholipids as a determinant of erythrocyte shape change: studies on electroporated cells. *Mol. Membr. Biol.* 16:247–255.

Schwarz, S., C. W. Haest, and B. Deuticke. 1999b. Extensive electroporation abolishes experimentally induced shape transformations of erythrocytes: a consequence of phospholipid symmetrization? *Biochim. Biophys. Acta.* 1421:361–379.

Sheetz, M. P. 1979. DNase-I-dependent dissociation of erythrocyte cytoskeletons. *J. Cell Biol.* 81:266–270.

Sheetz, M. P., and S. J. Singer. 1974. Biological membranes as bilayer couples: a molecular mechanism of drug-erythrocyte interactions. *Proc. Natl. Acad. Sci. U.S.A.* 71:4457–4461.

Simons, K., and D. Toomre. 2000. Lipid rafts and signal transduction. *Nat. Rev. Mol. Cell Biol.* 1:31–39.

Smith, J. E., N. Mohandas, and S. B. Shohet. 1982. Interaction of amphipathic drugs with erythrocytes from various species. *Am. J. Vet. Res.* 43:1041–1048.

Steck, T. L. 1989. Cell Shape: Determinants, Regulation, and Regulatory Role. W. D. Stein and F. Bronner, editors. Academic Press, San Diego, CA. 205–246.

Stokke, B. T., A. Mikkelsen, and A. Elgsaeter. 1986. Spectrin, human erythrocyte shapes, and mechanochemical properties. *Biophys. J.* 49:319–327.

Strey, H., M. Peterson, and E. Sackmann. 1995. Measurement of erythrocyte membrane elasticity by flicker eigenmode decomposition. *Biophys. J.* 69:478–488.

Svetina, S., M. Brumen, and B. Žekš. 1985. Lipid bilayer elasticity and the bilayer couple interpretation of red cell shape transformations and lysis. *Stud. Biophys.* 110:177–187.

Svoboda, K., C. F. Schmidt, D. Branton, and S. M. Block. 1992. Conformation and elasticity of the isolated red blood cell membrane skeleton. *Biophys. J.* 63:784–793.

Waugh, R., and E. A. Evans. 1979. Thermoelasticity of red blood cell membrane. *Biophys. J.* 26:115–131.

Waugh, R. E. 1996. Elastic energy of curvature-driven bump formation on red blood cell membrane. *Biophys. J.* 70:1027–1035.

Waugh, R. E., and R. G. Bauserman. 1995. Physical measurements of bilayer-skeletal separation forces. *Ann. Biomed. Eng.* 23:308–321.

Weed, R. I., and B. Chailley. 1972. Calcium-pH interactions in the production of shape change in erythrocytes. *Nouv. Rev. Fr. Hémat.* 12:775–788.

Weed, R. I., and B. Chailley. 1973. Red Cell Shape: Physiology, Pathology, Ultrastructure. M. Bessis, R. I. Weed, and P. F. Leblond, editors. Springer-Verlag, Berlin.

Wiese, W., W. Harbich, and W. Helfrich. 1992. Budding of lipid bilayer vesicles and flat membranes. *J. Phys. Condens. Matter.* 4:1647–1657.

Wong, P. 1994. Mechanism of control of erythrocyte shape: a possible relationship to band 3. *J. Theor. Biol.* 171:197–205.

Wong, P. 1999. A basis of echinocytosis and stomatocytosis in the disc-sphere transformations of the erythrocyte. *J. Theor. Biol.* 196:343–361.

Wortis, M. 1998. Phospholipid-bilayer vesicle shapes and shape transformations: theory vs. experiment. *Biol. Skr. Dan. Vidensk. Selsk.* 49:59–63.

Wortis, M., M. Jarić, and U. Seifert. 1997. Thermal shape fluctuations of fluid-phase phospholipid-bilayer membranes and vesicles. *J. Mol. Liq.* 71:195–207.

Zarda, P. R., S. Chien, and R. Skalak. 1977. Elastic deformations of red blood cells. *J. Biomech.* 10:211–221.